Computing manuscript No.
(will be inserted by the editor)

Numerical simulation of fluid-structure interaction of compressible flow and elastic structure

Jaroslava Hasnedlová · Miloslav Feistauer · Jaromír Horáček · Adam Kosík · Václav Kučera

Received: date / Accepted: date

Abstract The paper will be concerned with fluid-structure interaction problem of compressible flow and elastic structure in 2D domains with a special interest in medical applications to airflow in human vocal folds. The viscous flow in a time dependent domain is described by the Navier-Stokes equations written with the aid of the Arbitrary Lagrangian-Eulerian (ALE) method. The equations of motion for elastic deformations of the human vocal folds are coupled with the equations for the fluid flow using either loose or strong coupling. The space discretization of the flow problem is carried out by the discontinuous Galerkin finite element method. For the time discretization we use a semi-implicit scheme. In order to derive the space-time discretization of

Jaroslava Hasnedlová
Department of Numerical Mathematics, Faculty of Mathematics and Physics, Charles University, Sokolovská 83, 18675 Praha 8
Tel.: +420 732287764
Fax: +420 224811036
E-mail: jarkaprokop@post.cz

Miloslav Feistauer
Department of Numerical Mathematics, Faculty of Mathematics and Physics, Charles University, Sokolovská 83, 18675 Praha 8
E-mail: feist@karlin.mff.cuni.cz

Jaromr Horáček
Institute of Thermomechanics, The Academy of Sciences of the Czech Republic, v. v. i., Dolejškova 1402/5, 182 00 Praha 8
E-mail: jaromirh@it.cas.cz

Adam Kosík
Department of Numerical Mathematics, Faculty of Mathematics and Physics, Charles University, Sokolovská 83, 18675 Praha 8
E-mail: adam.kosik@atlas.cz

Václav Kučera
Department of Numerical Mathematics, Faculty of Mathematics and Physics, Charles University, Sokolovská 83, 18675 Praha 8
E-mail: kucera@karlin.mff.cuni.cz

the elastic body problem, we apply the finite element method using continuous piecewise linear elements. For the time discretization we use the Newmark scheme. Results of numerical experiments are presented.

Keywords fluid-structure interaction · compressible flow · ALE method · discontinuous Galerkin finite element method · coupling algorithms

Mathematics Subject Classification (2000) 74F10 · 65M60 · 65M12

1 Introduction

At the current speed of technology progress, the coupled problems describing the interaction of fluid flow with elastic structure motion are of great importance in many fields of physical and technical sciences such as biomechanics, aerospace, civil and mechanical engineering, etc.. The need of the modeling of flow around flexible structures leads to the developement of a new scientifical and technical discipline: the aeroelasticity. The aeroelasticity has many important engineering and scientific applications (e.g. in aerospace industry - aircraft design and safety; in civil engineering - stability of bridges, towers, smokestacks or skyscrapers; in mechanical engineering - bladed machines, etc.). The consequence of the aeroelastic effects can positively (the flow-induced vibration producing voice in human vocal folds) or negatively (the flow-induced vibration leading to material fatigue or inducing excessive noise generation) affect the operation of the system. The problems of the interaction of fluid flow with elastic structures were studied by a number of different methods in several books (e.g. [1], [2], [3], [4], [5], [6], [7]). Mostly, simplified linearized problems applied in technology are used. Recently, the research focuses also on mathematical and numerical modeling of nonlinear coupled problems. This represents complicated mathematical problems caused by the time-dependence of the computational domain and by the necessity of coupling of the flow problem with the elasticity problem. Here, we can mention for example the papers [8], [9], [10], [11]. In the case of overcoming the problems of coupling elasticity of the body with the flow problem we need to solve difficulties linked with the simulation of compressible flow. Due to the simulation of compressible flow in the time dependent domain, which is affected by the behaviour of the elastic structure, it is necessary to treat problems caused by nonlinear convection dominating over diffusion, i.e. boundary layers and wakes for large Reynolds numbers and instabilities caused by acoustic effects for low Mach numbers. A suitable numerical method for the solution of compressible flow suffering from mentioned difficulties is the discontinuous Galerkin finite element (DGFE) method.

The paper is devoted to the numerical simulation of fluid-structure interaction. Especially we are focused on the modeling of flow-induced vibrations of the human vocal folds during the phonation onset. It means that we need to take into account the simulation of compressible viscous flow in a time-dependent domain together with the elasticity behaviour of the channel walls formed by an elastic structure.

Our goal is the numerical finite element simulation of the interaction of 2D compressible viscous flow in the glottal region with a compliant tissue of the human vocal folds modeled by a 2D elastic layered structure. A question is the mathematical and physical description of the mechanism for transforming the airflow energy in the glottis into the acoustic energy representing the voice source in humans. The primary voice source is given by the airflow coming from the lungs that causes self-oscillations of the vocal folds. The voice source signal travels from the glottis to the mouth, exciting the acoustic supraglottal spaces, and becomes modified by acoustic resonance properties of the vocal tract ([12]).

In [13] we can find an overview of the current state of mathematical models for the human phonation process. Such models are valuable tools for providing insight into the basic mechanisms of phonation and in future could help with surgical planning, diagnostics and voice rehabilitation. In current publications various simplified glottal flow models are used. They are based on the Bernoulli equation ([12]), 1D models for an incompressible inviscid fluid ([14]), 2D incompressible Navier-Stokes equations solved by the finite volume method ([15]) or finite element method ([16]). Acoustic wave propagation in the vocal tract is usually modeled separately using linear acoustic perturbation theory ([17]). Also the work [18], which is concerned with the finite volume solution of the Navier-Stokes equations for a compressible fluid with prescribed periodic changes of the channel cross-section of the glottal channel, can be found. The phonation onset was studied by using the potential flow model and three-mass lumped model for the vibrating vocal folds in [19] and for a 2D isotropic elastic model of the vocal folds in [20].

In our case the flow problem is discretized in space by the discontinuous Galerkin finite element method, using piecewise polynomial approximations, in general discontinuous on interfaces between neighbouring elements. The time discretization is carried out by the backward difference formula (BDF) in time. The structural problem is approximated by conforming finite elements and the Newmark method. The fluid-structure interaction is realized via weak or strong coupling algorithms. The presented results of the numerical simulations show the convergence tendencies of the developed schemes, comparison of the influence of coupling algorithms and the long-time behaviour of the fluid-structure system.

2 Continuous problem

In this section we shall focus on the problem of the interaction of a compressible flow with an elastic structure.

2.1 Formulation of the flow problem

We consider a compressible flow in a bounded domain $\Omega_t \subset I\!R^2$ depending on time $t \in [0, T]$. We assume that the boundary of Ω_t is formed by three disjoint

parts: $\partial\Omega_t = \Gamma_I \cup \Gamma_O \cup \Gamma_{W_t}$, where Γ_I is the inlet, Γ_O is the outlet and Γ_{W_t} denotes impermeable walls that may move in dependence on time.

The dependence of the domain Ω_t on time is taken into account with the use of the *arbitrary Lagrangian-Eulerian* (ALE) method, see e.g. [21]. It is based on a regular one-to-one ALE mapping of the reference configuration Ω_0 onto the current configuration Ω_t:

$$\mathcal{A}_t : \overline{\Omega}_0 \longrightarrow \overline{\Omega}_t, \ \textit{i.e.}\ \boldsymbol{X} \in \overline{\Omega}_0 \longmapsto \boldsymbol{x} = \boldsymbol{x}(\boldsymbol{X}, t) = \mathcal{A}_t(\boldsymbol{X}) \in \overline{\Omega}_t. \tag{1}$$

We define the domain velocity:

$$\begin{aligned} \tilde{\boldsymbol{z}}(\boldsymbol{X}, t) &= \frac{\partial}{\partial t}\mathcal{A}_t(\boldsymbol{X}), \quad t \in [0, T], \ \boldsymbol{X} \in \Omega_0, \\ \boldsymbol{z}(\boldsymbol{x}, t) &= \tilde{\boldsymbol{z}}(\mathcal{A}^{-1}(\boldsymbol{x}), t), \quad t \in [0, T], \ \boldsymbol{x} \in \Omega_t, \end{aligned} \tag{2}$$

and the ALE derivative of a vector function $\boldsymbol{w} = \boldsymbol{w}(\boldsymbol{x}, t), \ \boldsymbol{w} = (w_1, \dots, w_4)^T$, defined for $\boldsymbol{x} \in \Omega_t$ and $t \in [0, T]$:

$$\frac{D^A}{Dt}\boldsymbol{w}(\boldsymbol{x}, t) = \frac{\partial \tilde{\boldsymbol{w}}}{\partial t}(\boldsymbol{X}, t), \tag{3}$$

where

$$\tilde{\boldsymbol{w}}(\boldsymbol{X}, t) = \boldsymbol{w}(\mathcal{A}_t(\boldsymbol{X}), t), \ \boldsymbol{X} \in \Omega_0, \ \boldsymbol{x} = \mathcal{A}_t(\boldsymbol{X}). \tag{4}$$

Then, using the relations

$$\frac{D^A w_i}{Dt} = \frac{\partial w_i}{\partial t} + \operatorname{div}(\boldsymbol{z} w_i) - w_i \operatorname{div} \boldsymbol{z}, \quad i = 1, \dots, 4, \tag{5}$$

we can write the governing system consisting of the continuity equation, the Navier-Stokes equations and the energy equation in the ALE form

$$\frac{D^A \boldsymbol{w}}{Dt} + \sum_{s=1}^{2} \frac{\partial \boldsymbol{g}_s(\boldsymbol{w})}{\partial x_s} + \boldsymbol{w} \operatorname{div} \boldsymbol{z} = \sum_{s=1}^{2} \frac{\partial \boldsymbol{R}_s(\boldsymbol{w}, \nabla \boldsymbol{w})}{\partial x_s}. \tag{6}$$

See, for example [22]. Here

$$\begin{aligned} \boldsymbol{w} &= (w_1, \dots, w_4)^T = (\rho, \rho v_1, \rho v_2, E)^T \in I\!R^4, \\ \boldsymbol{w} &= \boldsymbol{w}(\boldsymbol{x}, t), \ \boldsymbol{x} \in \Omega_t, \ t \in (0, T), \\ \boldsymbol{g}_s(\boldsymbol{w}) &= \boldsymbol{f}_s(\boldsymbol{w}) - z_s \boldsymbol{w}, \quad s = 1, 2, \\ \boldsymbol{f}_i(\boldsymbol{w}) &= (f_{i1}, \cdots, f_{i4})^T = \left(\rho v_i, \rho v_1 v_i + \delta_{1i}\, p, \rho v_2 v_i + \delta_{2i}\, p, (E + p) v_i\right)^T, \\ \boldsymbol{R}_i(\boldsymbol{w}, \nabla \boldsymbol{w}) &= (R_{i1}, \dots, R_{i4})^T = \left(0, \tau_{i1}^V, \tau_{i2}^V, \tau_{i1}^V\, v_1 + \tau_{i2}^V\, v_2 + k \partial\theta/\partial x_i\right)^T, \\ \tau_{ij}^V &= \lambda \operatorname{div} \boldsymbol{v}\, \delta_{ij} + 2\mu\, d_{ij}(\boldsymbol{v}), \ d_{ij}(\boldsymbol{v}) = \frac{1}{2}\left(\frac{\partial v_i}{\partial x_j} + \frac{\partial v_j}{\partial x_i}\right). \end{aligned} \tag{7}$$

We use the following notation: ρ – density, p – pressure, E – total energy, $\boldsymbol{v} = (v_1, v_2)$ – velocity, θ – absolute temperature, $\gamma > 1$ – Poisson adiabatic constant, $c_v > 0$ – specific heat at constant volume, $\mu > 0, \lambda = -2\mu/3$ – viscosity coefficients, k – heat conduction, τ_{ij}^V – components of the viscous

part of the stress tensor. The vector-valued function $\boldsymbol{w}$ is called state vector, the functions $\boldsymbol{f}_i$ are the so-called inviscid fluxes and $\boldsymbol{R}_i$ represent viscous terms. The above system is completed by the thermodynamical relations

$$p = (\gamma - 1)(E - \rho|\boldsymbol{v}|^2/2), \quad \theta = \left(\frac{E}{\rho} - \frac{1}{2}|\boldsymbol{v}|^2\right)/c_v. \tag{8}$$

The resulting system is equipped with the initial condition

$$\boldsymbol{w}(x,0) = \boldsymbol{w}^0(x), \quad \boldsymbol{x} \in \Omega_0, \tag{9}$$

and the following boundary conditions:

$$\begin{aligned}
&\text{a)}\ \ \rho|_{\Gamma_I} = \rho_D, \quad \text{b)}\ \ \boldsymbol{v}|_{\Gamma_I} = \boldsymbol{v}_D = (v_{D1}, v_{D2})^{\mathrm{T}}, \\
&\text{c)}\ \ \sum_{i,j=1}^{2} \tau_{ij}^V n_i v_j + k\frac{\partial \theta}{\partial n} = 0 \quad \text{on } \Gamma_I, \\
&\text{d)}\ \ \boldsymbol{v} = \boldsymbol{z}_D = \text{velocity of a moving wall}, \ \text{e)}\ \ \frac{\partial \theta}{\partial n} = 0 \text{ on } \Gamma_{W_t}, \\
&\text{f)}\ \ \sum_{i=1}^{2} \tau_{ij}^V n_i = 0, \quad j = 1,\, 2, \quad \text{g)}\ \ \frac{\partial \theta}{\partial n} = 0 \text{ on } \Gamma_O.
\end{aligned} \tag{10}$$

2.2 Elasticity problem and fluid-structure interaction coupling

For the description of the deformation of an elastic structure we shall use the model of dynamical linear elasticity formulated in a bounded open set $\Omega^b \subset I\!R^2$ representing the elastic body, which has a common boundary with the reference domain Ω_0 occupied by the fluid at the initial time. We denote by $\boldsymbol{u}(\boldsymbol{X}, t) = (u_1(\boldsymbol{X}, t), u_2(\boldsymbol{X}, t)$, $\boldsymbol{X} = (X_1, X_2) \in \Omega^b$, $t \in (0, T)$, the displacement of the body. The equations describing the deformation of the elastic body Ω^b have the form

$$\varrho^b \frac{\partial^2 u_i}{\partial t^2} + C\varrho^b \frac{\partial u_i}{\partial t} - \sum_{j=1}^{2} \frac{\partial \tau_{ij}^b}{\partial X_j} = 0, \quad \text{in } \Omega^b \times (0,T), \quad i = 1, 2. \tag{11}$$

Here τ_{ij}^b are the components of the stress tensor defined by the generalized Hooke's law for isotropic bodies

$$\tau_{ij}^b = \lambda^b \mathrm{div}\, \boldsymbol{u}\delta_{ij} + 2\mu^b e_{ij}^b, \quad i, j = 1, 2. \tag{12}$$

By $\boldsymbol{e}^b = \{e_{ij}^b\}_{i,j=1}^2$ we denote the strain tensor defined by

$$e_{ij}^b(\boldsymbol{u}) = \frac{1}{2}\left(\frac{\partial u_i}{\partial X_j} + \frac{\partial u_j}{\partial X_i}\right), \quad i, j = 1, 2. \tag{13}$$

The Lamé coefficients λ^b and μ^b are related to the Young modulus E^b and to the Poisson ratio σ^b as

$$\lambda^b = \frac{E^b \sigma^b}{(1+\sigma^b)(1-2\sigma^b)}, \quad \mu^b = \frac{E^b}{2(1+\sigma^b)}. \tag{14}$$

The expression $C\varrho^b \frac{\partial u_i}{\partial t}$, where $C \geq 0$, is the dissipative structural damping of the system and ϱ^b denotes the material density.

We complete the elasticity problem by initial and boundary conditions. The initial conditions read

$$\boldsymbol{u}(\cdot, 0) = 0, \quad \frac{\partial \boldsymbol{u}}{\partial t}(\cdot, 0) = 0 \quad \text{in } \Omega^b. \tag{15}$$

Further, we assume that $\partial\Omega^b = \Gamma_W^b \cup \Gamma_D^b$, where Γ_W^b and Γ_D^b are two disjoints parts of $\partial\Omega^b$. We assume that Γ_W^b is a common part between the fluid and structure at time $t = 0$. This means that $\Gamma_W^b \subset \Gamma_{W_0}$. On Γ_W^b we prescribe the normal component of the stress tensor and assume that the part Γ_D^b is fixed. This means that the following boundary conditions are used:

$$\sum_{j=1}^{2} \tau_{ij}^b n_j = T_i^{\boldsymbol{n}} \quad \text{on } \Gamma_W^b \times (0,T), \qquad i = 1,2, \tag{16}$$

$$\boldsymbol{u} = 0 \quad \text{on } \Gamma_D^b \times (0,T). \tag{17}$$

By $T_i^{\boldsymbol{n}}$, $i = 1,2$, we denote the prescribed normal components of the stress tensor and $\boldsymbol{n}(\boldsymbol{X}) = (n_1(\boldsymbol{X}), n_2(\boldsymbol{X}))$ denotes the unit outer normal to the body Ω^b on Γ_W^b at the point $\boldsymbol{X}$.

The structural problem consists in finding the displacement $\boldsymbol{u}$ satisfying equation (11) and the initial and boundary conditions (15) - (17).

Now we shall deal with the formulation of the coupled FSI problem. We denote the common boundary between the fluid and the structure at time t by $\tilde{\Gamma}_{W_t}$. It is given by

$$\tilde{\Gamma}_{W_t} = \left\{ \boldsymbol{x} \in I\!R^2;\ \boldsymbol{x} = \boldsymbol{X} + \boldsymbol{u}(\boldsymbol{X}, t),\ \boldsymbol{X} \in \Gamma_W^b \right\}. \tag{18}$$

This means that the domain Ω_t is determined by the displacement $\boldsymbol{u}$ of the part Γ_W^b at time t. The ALE mapping $\mathcal{A}_t$ is constructed with the aid of a special stationary linear elasticity problem - see Section 4.1.

If the domain Ω_t occupied by the fluid at time t is known, we can solve the problem describing the flow and compute the surface force acting on the body on the part $\tilde{\Gamma}_{W_t}$, which can be transformed to the reference configuration, i.e. to the interface Γ_W^b. In case of the linear elasticity model, when only small deformations are considered, we get the transmission conditions

$$\sum_{j=1}^{2} \tau_{ij}^b(\boldsymbol{X}) n_j(\boldsymbol{X}) = -\sum_{j=1}^{2} \tau_{ij}^f(\boldsymbol{x}) n_j(\boldsymbol{X}), \quad i = 1,2, \tag{19}$$

where τ_{ij}^f are the components of the stress tensor of the fluid:

$$\tau_{ij}^f = -p\delta_{ij} + \tau_{ij}^V, \quad i,j = 1,2. \tag{20}$$

The points $\boldsymbol{x}$ and $\boldsymbol{X}$ satisfy the relation

$$\boldsymbol{x} = \boldsymbol{X} + \boldsymbol{u}(\boldsymbol{X},t). \tag{21}$$

Further, the fluid velocity is defined on the moving part of the boundary $\tilde{\Gamma}_{W_t}$ by the second transmission condition

$$\boldsymbol{v}(\boldsymbol{x},t) = \boldsymbol{z}_D(\boldsymbol{x},t) = \frac{\partial \boldsymbol{u}(\boldsymbol{X},t)}{\partial t}. \tag{22}$$

Finally, we formulate the *continuous FSI problem*: We want to determine the domain Ω_t, $t \in (0,T]$ and functions $\boldsymbol{w} = \boldsymbol{w}(\boldsymbol{x},t)$, $\boldsymbol{x} \in \overline{\Omega}_t$, $t \in [0,T]$ and $\boldsymbol{u} = \boldsymbol{u}(\boldsymbol{X},t)$, $\boldsymbol{X} \in \overline{\Omega}^b$, $t \in [0,T]$ satisfying equations (6), (11), the initial conditions (9), (15), the boundary conditions (10), (16), (17) and the transmission conditions (19), (22).

This FSI problem is strongly nonlinear. In the sequel we shall be concerned with its numerical solution.

3 Discrete problem

This part will be devoted to the description of the numerical methods used for the solution of the separately considered flow and structural model.

3.1 Discretization of the flow problem

For the space semidiscretization of the flow problem we use the discontinuous Galerkin finite element method (DGFEM).

We construct a polygonal approximation Ω_{ht} of the domain Ω_t. By $\mathcal{T}_{ht}$ we denote a partition of the closure $\bar{\Omega}_{ht}$ of the domain Ω_{ht} into a finite number of closed triangles K with mutually disjoint interiors such that $\bar{\Omega}_{ht} = \bigcup_{K\in\mathcal{T}_{ht}} K$. The approximate solution will be sought in the space of piecewise polynomial functions

$$\boldsymbol{S}_{ht} = [S_{ht}]^4 \quad \text{with } S_{ht} = \{v; v|_K \in P^r(K)\ \forall\, K \in \mathcal{T}_{ht}\}, \tag{23}$$

where $r \geq 1$ is an integer and $P^r(K)$ denotes the space of all polynomials on K of degree $\leq r$. A function $\boldsymbol{\varphi} \in \boldsymbol{S}_{ht}$ is, in general, discontinuous on interior faces of the triangulation.

The discrete problem is derived in the following way: We multiply system (6) by a test function $\boldsymbol{\varphi}_h \in \boldsymbol{S}_{ht}$, integrate over $K \in \mathcal{T}_{ht}$, apply Green's theorem, sum over all elements $K \in \mathcal{T}_{ht}$, use the concept of the numerical flux and introduce suitable terms mutually cancelling for a regular exact solution. Moreover, we carry out a linearization of the nonlinear terms. Then, the semidiscrete

solution of problem (6) is defined as a function $\boldsymbol{w}_h \in C^1((0,T), \boldsymbol{S}_{ht})$ fulfilling the conditions

$$\int_{\Omega_{ht}} \frac{D^{\mathcal{A}}\boldsymbol{w}_h}{Dt}(t) \cdot \boldsymbol{\varphi}_h \, d\boldsymbol{x} + d_h(\boldsymbol{w}_h(t), \boldsymbol{\varphi}_h) + b_h(\boldsymbol{w}_h(t), \boldsymbol{\varphi}_h) \tag{24}$$
$$+a_h(\boldsymbol{w}_h(t), \boldsymbol{\varphi}_h) + J_h(\boldsymbol{w}_h(t), \boldsymbol{\varphi}_h) = l_h(\boldsymbol{w}_h(t), \boldsymbol{\varphi}_h) \quad \forall \boldsymbol{\varphi}_h \in \boldsymbol{S}_{ht}, \ \forall t \in (0,T),$$
$$\boldsymbol{w}_h(0) = \boldsymbol{w}_h^0, \tag{25}$$

where $\boldsymbol{w}_h^0$ is the $L^2(\Omega_{h0})$-projection of $\boldsymbol{w}^0$ on $\boldsymbol{S}_{h0}$. This means that

$$\left(\boldsymbol{w}_h^0, \boldsymbol{\varphi}_h\right) = \left(\boldsymbol{w}^0, \boldsymbol{\varphi}_h\right) \quad \forall \boldsymbol{\varphi}_h \in \boldsymbol{S}_{h0}. \tag{26}$$

For a detailed description of the whole process and the definition of the forms appearing in (24), see [22].

Because of the time discretization of (24) we construct a partition $0 = t_0 < t_1 < t_2 \ldots$ of the time interval $[0,T]$ and define the time step $\tau_k = t_{k+1} - t_k$. We use the approximations $\boldsymbol{w}_h(t_n) \approx \boldsymbol{w}_h^n \in \boldsymbol{S}_{ht_n}$, $\boldsymbol{z}(t_n) \approx \boldsymbol{z}^n$, $n = 0, 1, \ldots$, and introduce the function $\hat{\boldsymbol{w}}_h^k = \boldsymbol{w}_h^k \circ \mathcal{A}_{t_k} \circ \mathcal{A}_{t_{k+1}}^{-1}$, which is defined in the domain $\Omega_{ht_{k+1}}$. The ALE derivative at time t_{k+1} is approximated by the first-order backward finite difference

$$\frac{D^A\boldsymbol{w}_h}{Dt}(\boldsymbol{x}, t_{k+1}) \approx \frac{\boldsymbol{w}_h^{k+1}(\boldsymbol{x}) - \hat{\boldsymbol{w}}_h^k(\boldsymbol{x})}{\tau_k}, \quad \boldsymbol{x} \in \Omega_{ht_{k+1}}. \tag{27}$$

The remaining terms are treated with the aid of a partial linearization and extrapolation in nonlinear terms. For details see [22].

3.2 Discretization of the structural problem

The space semidiscretization of the structural problem is carried out by the conforming finite element method. By Ω_h^b we denote a polygonal approximation of the domain Ω^b. We construct a triangulation $\mathcal{T}_h^b$ of the domain Ω_h^b formed by a finite number of closed triangles. Then the approximate solution of the structural problem is sought in the finite-dimensional space $\boldsymbol{X}_h = X_h \times X_h$, where

$$X_h = \left\{ v_h \in C(\bar{\Omega}_h^b); \ v_h|_K \in P^s(K), \ \forall K \in \mathcal{T}_h^b \right\}. \tag{28}$$

Here $s \geq 1$ is an integer. In $\boldsymbol{X}_h$ we define the subspace $\boldsymbol{V}_h = V_h \times V_h$, where

$$V_h = \left\{ y_h \in X_h; y_h|_{\bar{\Gamma}_{Dh}^b} = 0 \right\}. \tag{29}$$

The derivation of the space semidiscretization can be obtained in a standard way by multiplying system (11) by any test function $y_{hi} \in V_h$, $i = 1, 2$, applying Green's theorem and using the boundary condition (16). Using the

notation $\boldsymbol{u}_h'(t) = \frac{\partial \boldsymbol{u}_h(t)}{\partial t}$, $\boldsymbol{u}_h''(t) = \frac{\partial^2 \boldsymbol{u}_h(t)}{\partial t^2}$, $T^{\boldsymbol{n}} = (T_1^{\boldsymbol{n}}, T_2^{\boldsymbol{n}})$ and defining the form

$$a_h(\boldsymbol{u}_h, \boldsymbol{y}_h) = \int_{\Omega_h^b} \lambda^b \mathrm{div}\, \boldsymbol{u}_h \,\mathrm{div}\, \boldsymbol{y}_h \, d\boldsymbol{X} \tag{30}$$
$$+2 \int_{\Omega_h^b} \mu^b \sum_{i,j=1}^{2} e_{ij}^b(\boldsymbol{u}_h)\, e_{ij}^b(\boldsymbol{y}_h)\, d\boldsymbol{X},$$

we define the approximate solution of the structural problem as a function $t \in [0,T] \to \boldsymbol{u}_h(t) \in \boldsymbol{V}_h$ such that there exist derivatives $\boldsymbol{u}_h'(t)$, $\boldsymbol{u}_h''(t)$ and the identity

$$\int_{\Omega_h^b} \rho^b \boldsymbol{u}_h''(t) \cdot \boldsymbol{y}_h \, d\boldsymbol{X} + C \int_{\Omega_h^b} \rho^b \boldsymbol{u}_h'(t) \cdot \boldsymbol{y}_h \, d\boldsymbol{X} + a(\boldsymbol{u}_h(t), \boldsymbol{y}_h) \tag{31}$$
$$= \int_{\Gamma_{Wh}} T_h^{\boldsymbol{n}}(t) \cdot \boldsymbol{y}_h \, dS_{\boldsymbol{X}}, \quad \forall \boldsymbol{y}_h \in \boldsymbol{V}_h, \quad \forall t \in (0,T),$$

and the initial conditions

$$\boldsymbol{u}_h(\boldsymbol{X}, 0) = 0, \quad \boldsymbol{u}_h'(\boldsymbol{X}, 0) = 0, \quad \boldsymbol{X} \in \Omega_h^b, \tag{32}$$

are satisfied. This approach leads to a system of ordinary differential equations. The time discretization is carried out by the Newmark method.

4 Realization of the coupled FSI problem

In this section we shall describe the algorithm of the numerical realization of the complete fluid-structure interaction problem.

4.1 Construction of the ALE mapping for fluid

The ALE mapping is constructed with the aid of an artificial stationary elasticity problem. We seek $\boldsymbol{d} = (d_1, d_2)$ defined in Ω_0 as a solution of the elastostatic system

$$\sum_{j=1}^{2} \frac{\partial \tau_{ij}^a}{\partial x_j} = 0 \quad \text{in } \Omega_0, \quad i = 1,2, \tag{33}$$

where τ_{ij}^a are the components of the artificial stress tensor

$$\tau_{ij}^a = \lambda^a \mathrm{div}\, \boldsymbol{d} \delta_{ij} + 2\mu^a e_{ij}^a, \quad e_{ij}^a(\boldsymbol{d}) = \frac{1}{2}\left(\frac{\partial d_i}{\partial x_j} + \frac{\partial d_j}{\partial x_i}\right), \quad i,j = 1,2. \tag{34}$$

The Lamé coefficients λ^a and μ^a are related to the artificial Young modulus E^a and to the artificial Poisson number σ_a as in (14). The boundary conditions for $\boldsymbol{d}$ are prescribed by

$$\boldsymbol{d}|_{\Gamma_I \cup \Gamma_O} = 0, \ \boldsymbol{d}|_{\Gamma_{W_0 h} \setminus \Gamma_{Wh}} = 0, \ \boldsymbol{d}(\boldsymbol{X}, t) = \boldsymbol{u}(\boldsymbol{X}, t), \ \boldsymbol{X} \in \Gamma_{Wh}. \tag{35}$$

The solution of (33) gives us the ALE mapping of $\overline{\Omega}_0$ onto $\overline{\Omega}_t$ in the form

$$\mathcal{A}_t(\boldsymbol{X}) = \boldsymbol{X} + \boldsymbol{d}(\boldsymbol{X}, t), \quad \boldsymbol{X} \in \overline{\Omega}_0, \tag{36}$$

for each time t.

System (33) is discretized by the conforming piecewise linear finite elements on the mesh $\mathcal{T}_{h0}$ used for computing the flow field in the beginning of the computational process in the polygonal approximation Ω_{h0} of the domain Ω_0.The use of linear finite elements is sufficient, because we need only to know the movement of the points of the mesh.

If the displacement $\boldsymbol{d}_h$ is computed at time t_{k+1}, then in view of (36), the approximation of the ALE mapping is obtained in the form

$$\mathcal{A}_{t_{k+1}h}(\boldsymbol{X}) = \boldsymbol{X} + \boldsymbol{d}_h(\boldsymbol{X}), \quad \boldsymbol{X} \in \Omega_{0h}. \tag{37}$$

The knowledge of the ALE mapping at the time instants t_k, t_{k+1} allows us to approximate the domain velocity with the aid of the first-order backward difference formula.

4.2 Coupling procedure

In the solution of the complete coupled fluid-structure interaction problem it is necessary to apply a suitable coupling procedure. The general framework can be found, e.g. in [23]. In our case we apply two different types of algorithms.

First, we present the *weak coupling* algorithm:

1. Compute the approximate solution of the flow problem (6) on the time level t_m.
2. Compute the corresponding stress tensor of the fluid τ_{ij}^f and the aerodynamical force acting on the structure and transform it to the interface Γ_{Wh}^b by (19).
3. Solve the elasticity problem (31) - (32) and compute the deformation $\boldsymbol{u}_{h,m}$ at time t_m. On the basis of (18) set

$$\tilde{\Gamma}_{W_{t_{k+1}}} = \{\boldsymbol{x} = \boldsymbol{X} + \boldsymbol{u}_{h,m}(\boldsymbol{X});\ \boldsymbol{X} \in \Gamma_W^b\}, \tag{38}$$

   and determine the domain $\Omega_{ht_{m+1}}$.
4. Determine the ALE mapping $\mathcal{A}_{t_{m+1}h}$ by (33) and approximate the domain velocity $\boldsymbol{z}_{h,m+1}$.
5. Set $m := m + 1$, go to 1).

The *strong coupling* procedure represents a more complicated algorithm. It follows this outline:

1. Assume that the approximate solution $\boldsymbol{w}_h^m$ of the flow problem and the deformation $\boldsymbol{u}_{h,m}$ of the structure are known on the time level t_m.
2. Set $\boldsymbol{u}_{h,m+1}^0 := \boldsymbol{u}_{h,m},\ k := 1$ and apply the iterative process:

(a) Compute the stress tensor of the fluid τ_{ij}^f and the aerodynamical force acting on the structure and transform it to the interface Γ_{Wh}^b.
(b) Solve the elasticity problem, compute the approximation of the deformation $\boldsymbol{u}_{h,m+1}^k$ and construct the approximation $\Omega_{ht_{m+1}}^k$ of the flow domain at time t_{m+1}.
(c) Determine the approximations of the ALE mapping $\mathcal{A}_{t_{m+1}h}^k$ and the domain velocity $\boldsymbol{z}_{h,m+1}^k$.
(d) Solve the flow problem in $\Omega_{ht_{m+1}}^k$ and obtain the approximate solution $\boldsymbol{w}_{h,m+1}^k$.
(e) If the variation $|\boldsymbol{u}_{h,m+1}^k - \boldsymbol{u}_{h,m+1}^{k-1}|$ of the displacement is larger than the prescribed tolerance and $k < 50$, go to a) and $k := k+1$. Else $\Omega_{ht_{m+1}} := \Omega_{ht_m}^k$, $\boldsymbol{w}_h^{m+1} := \boldsymbol{w}_{h,m+1}^k$, $\boldsymbol{u}_h^{m+1} := \boldsymbol{u}_{h,m}^k$, $m := m+1$ and goto 2).

The difference between these two coupling algorithms is demonstrated by our numerical results in what follows.

5 Numerical experiments

We consider the model of flow through a channel with two bumps which represent time dependent boundaries between the flow and a simplified model of vocal folds (see Figure 1). The numerical experiments were carried out for

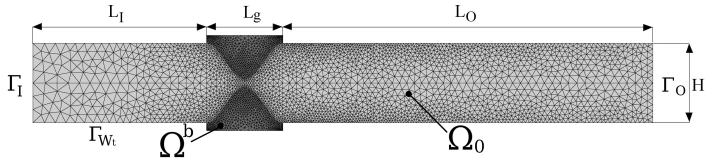

Fig. 1 Computational domain at time $t = 0$ with a finite element mesh and the description of its size: $L_I = 50$ mm, $L_g = 15.4$ mm, $L_O = 94.6$ mm, $H = 16$ mm. The width of the channel in the narrowest part is 1.6 mm.

the following data: magnitude of the inlet velocity $v_{in} = 4$ m/s, the viscosity $\mu = 15 \cdot 10^{-6}\,\mathrm{kg\,m^{-1}\,s^{-1}}$, the inlet fluid density $\rho_{in} = 1.225\,\mathrm{kg\,m^{-3}}$, the outlet pressure $p_{out} = 97611$ Pa, the Reynolds number $Re = \rho_{in} v_{in} H/\mu = 5227$, heat conduction coefficient $k = 2.428 \cdot 10^{-2}\,\mathrm{kg\,m\,s^{-2}\,K^{-1}}$, the specific heat $c_v = 721.428\,\mathrm{m^2\,s^{-2}\,K^{-1}}$, the Poisson adiabatic constant $\gamma = 1.4$. The inlet Mach number is $M_{in} = 0.012$. The parameter of the computational accuracy of the GMRES solver was 10^{-10}. The Young modulus and the Poisson ratio of the structure have the values $E^b = 25000$ Pa and $\sigma^b = 0.4$, respectively, the structural damping coefficient is equal to the constant $C = 100\ \mathrm{s^{-1}}$ and the material density $\rho^b = 1040\,\mathrm{kg\,m^{-3}}$. The artificial Young modulus $E^a = 10000$ and the Poisson ratio $\sigma^a = 0.45$. The used time step was $8 \cdot 10^{-6}$s.

Mesh	Line used in graphs	Flow part	Structure part
Mesh 1	solid line	5398	1998
Mesh 2	dashed line	10130	2806
Mesh 3	dotted line	20484	4076

Table 1 Computational meshes.

Time step	Line used in graphs	Size
Time step 1	solid line	$2 \cdot 10^{-6}$ s
Time step 2	dashed line	$4 \cdot 10^{-6}$ s
Time step 3	dotted line	$8 \cdot 10^{-6}$ s

Table 2 Used time steps.

In the numerical experiments quadratic ($r = 2$) and linear ($s = 1$) elements were used for the approximation of flow and structural problem, respectively.

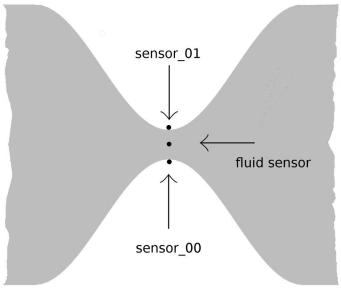

Fig. 2 Allocation of the sensors.

First we shall compare the influence of the density of three computational meshes on the total displacement at the point *sensor*_00 (see Figure 2). Table 1 contains the numbers of elements of the triangulations in the flow and structure domains. The choosen time step was $8 \cdot 10^{-6}$ s. The corresponding Fourier analyses are carried out by the software Matlab. Figure 3 shows the behaviour of the total displacement computed with the aid of the strong coupling. There are also presented corresponding Fourier analyses. The influence of the mesh density can be seen mainly in the graphs of the Fourier analyses of the solution of Figure 3. We can observe that the dominating frequencies in all cases are very close to each other.

Further we are interested in comparison of the influence of the time step size on the total displacement at the point *sensor*_00 (see Figure 2). Table 2 contains the chosen time steps. Again the total displacement and the corresponding Fourier analysis are presented. (see Figure 4). The computation was carried out for the mesh with 10130 elements in the flow part. In this case we can observe a good agreement of the results for all three different time steps.

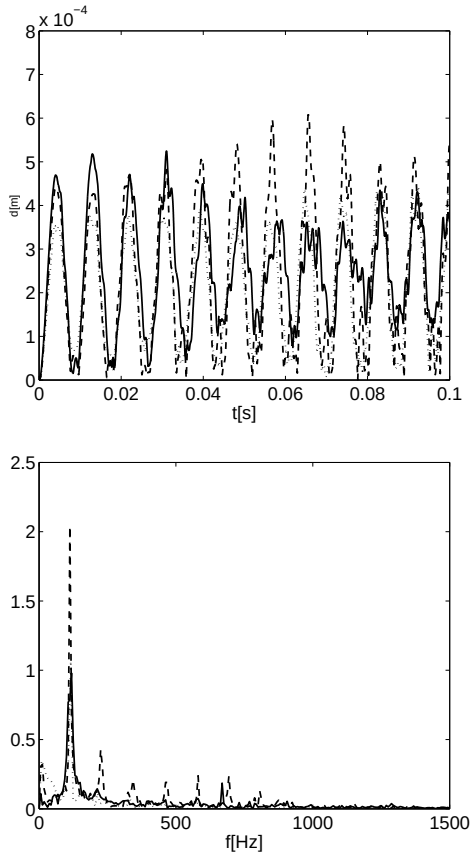

Fig. 3 Dependence of the total displacement on time and its Fourier analysis computed on three meshes.

In order to compare an impact of the used coupling procedures we present the graphs of the pressure amplitude

$$(p - p_{average})(t) = p(A,t) - \frac{1}{T}\int_0^T p(A,t)\mathrm{d}t \tag{39}$$

on the mesh 1 with time step $\tau = 2 \cdot 10^{-6}$ s computed by the strong coupling (solid line) and the weak coupling (dashed line). The position of the point A is seen in Figure 5. Figure 6 shows that the difference between the Fourier analyses obtained by the strong and weak coupling is not too large. The main difference is in a higher stability of the strong coupling during the calculation on a long time interval. On the other hand, the strong coupling requires naturally longer CPU time.

Now, let us deal with the flow field in the channel and the flow-induced deformations of the vocal folds model. In what follows, we shall present the results obtained by the computation on the coarse mesh (mesh 1 in Table

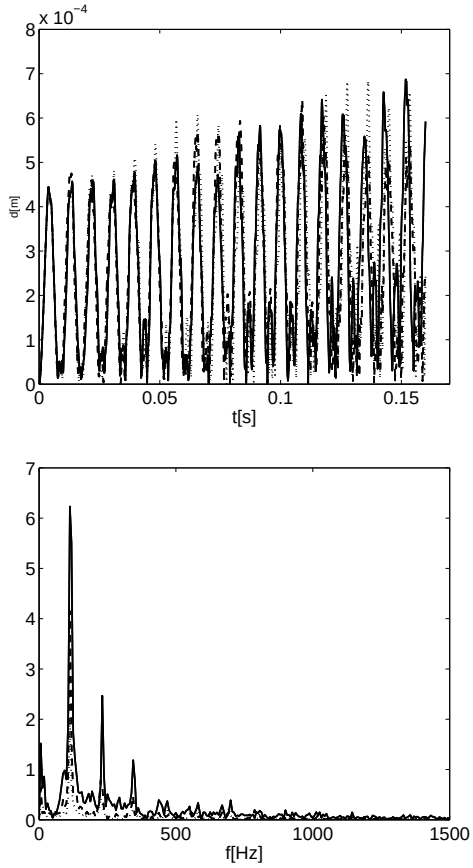

Fig. 4 Dependence of the total displacement on time and its Fourier analysis.

Fig. 5 Position of the point A in the flow channel, where the analysis of the convergence tendency was carried out.

1). The coarse mesh was chosen in order to allow us the computation on the long time interval in a reasonable time. The strong coupling was used. In Figures 7 and 8 we can see the computational mesh and the velocity field near the vocal folds at several time instants. Figures 9 and 10 show the pressure isolines and the velocity isolines in the whole channel at same time instants as in Figure 8. The maxima of the fluid velocity $v \approx 54$ ms^{-1} and the pressure 2 kPa correspond to the parameters of normal phonation. We can observe the Coanda effect represented by the attachment of the main stream (jet) successively to the upper and lower wall and formation of large scale vortices behind the glottis. The character of the vocal folds vibrations can be indicated

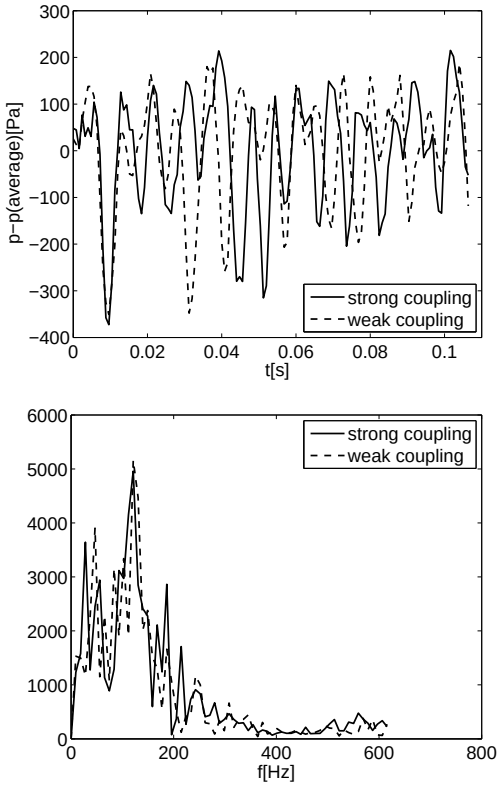

Fig. 6 Comparison of the time dependence of the pressure amplitude at the point A (above) and the Fourier analysis (below) obtained by the weak and strong coupling.

in Figure 11, which shows the displacements d_x and d_y of the sensor points on the vocal folds surface (marked in Figure 2) in the horizontal and vertical directions, respectively. Moreover, the fluid pressure fluctuations in the middle of the gap as well as the Fourier analysis of the signals are shown here too. The vocal folds vibrations are not fully symmetric due to the Coanda effect and are composed of the fundamental horizontal mode of vibration with the corresponding frequency 113 Hz and by the higher vertical mode with the frequency 439 Hz. The increase of vertical vibrations due to the aeroelastic instability of the system results in a fast decrease of the glottal gap. At about $t = 0.2$ s, when the gap is nearly closed, the fluid mesh deformation in this region is too high and the numerical simulation stopped. The dominant peak at 439 Hz in the spectrum of the pressure signal corresponds well to the vertical oscillations of the glottal gap, while the influence of the lower frequency 113 Hz associated with the horizontal vocal folds motion is in the pressure fluctuations negligible. The modeled flow-induced instability of the vocal folds is called phonation onset followed in reality by a complete closing of the glottis and consequently by the vocal folds collisions producing the voice acoustic signal.

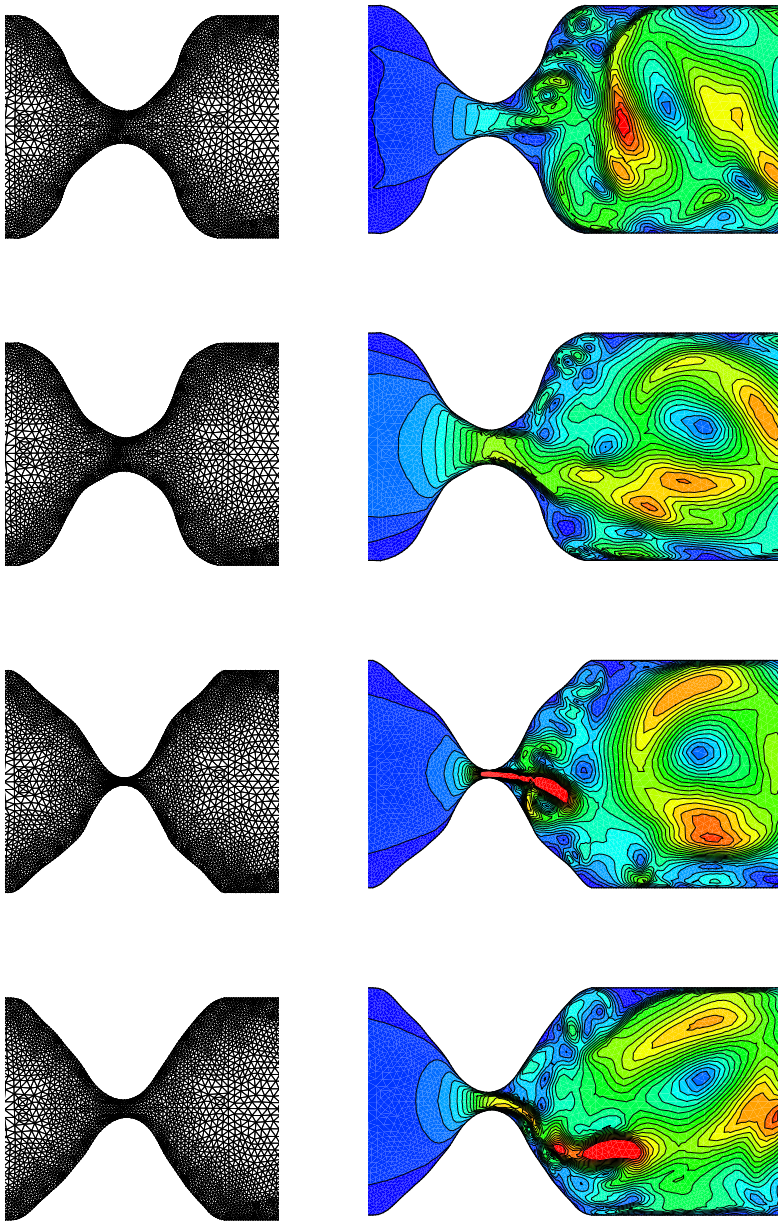

Fig. 7 Detail of the mesh and the velocity distribution in the vicinity of the narrowest part of the channel at time instants $t = 0.1950, 0.1957, 0.1963, 0.1970$ s.

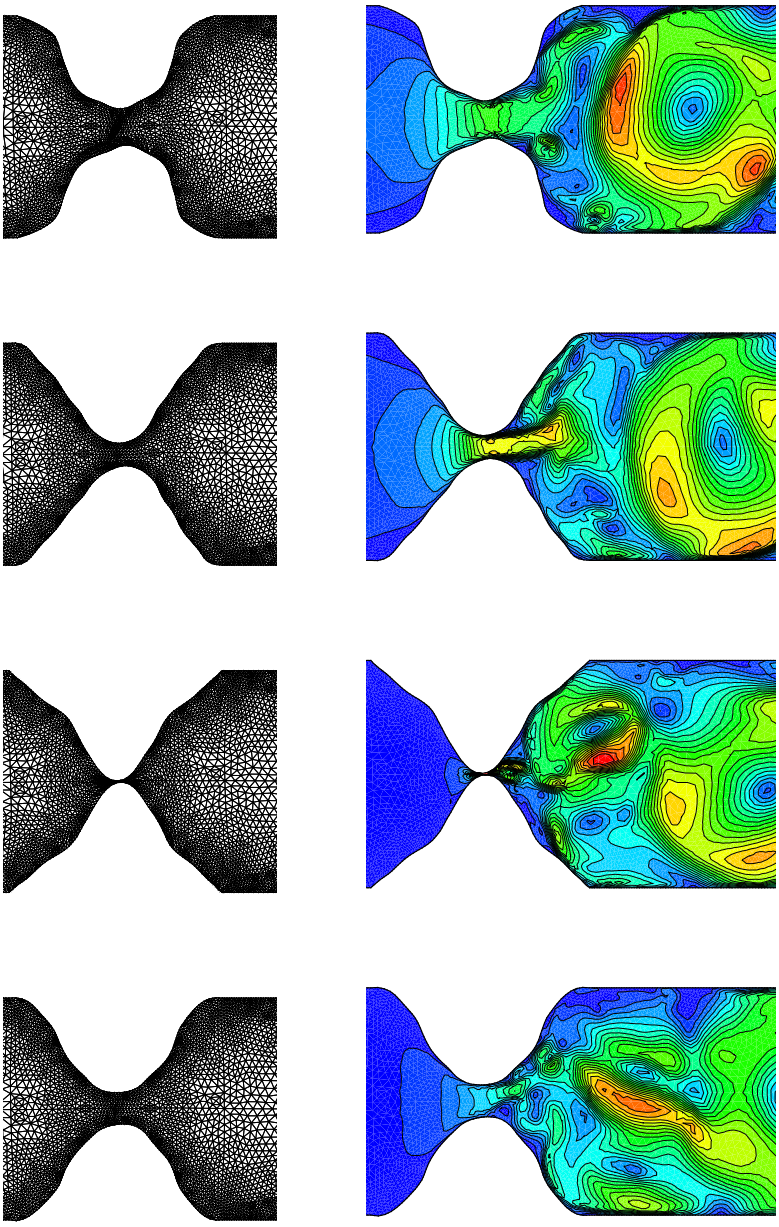

Fig. 8 Detail of the mesh and the velocity distribution in the vicinity of the narrowest part of the channel at time instants $t = 0.1976, 0.1982, 0.1989, 0.1995$ s.

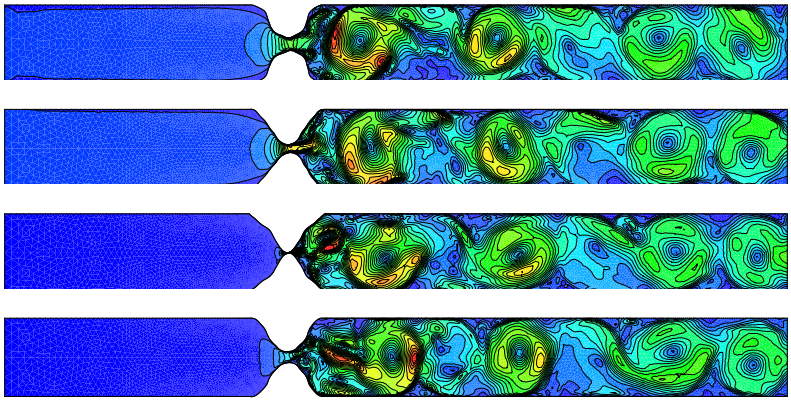

Fig. 9 Velocity isolines at time instants $t = 0.1976, 0.1982, 0.1989, 0.1995$ s.

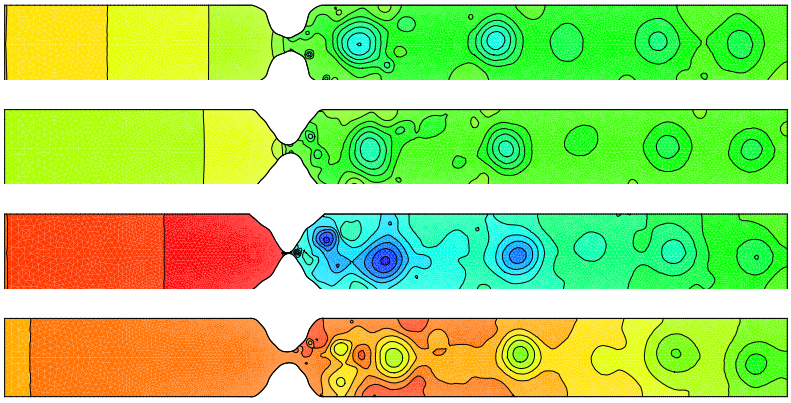

Fig. 10 Isolines of the field $p - p_{out}$ (pressure related to the outlet value) at time instants $t = 0.1976, 0.1982, 0.1989, 0.1995$ s.

6 Conclusion

As seen from our numerical experiments, we have presented a robust method for the numerical simulation of the interaction of compressible flow with elastic structure with applications to the computation of flow-induced vibrations of vocal folds during phonation onset.

Future work should be concentrated on the realization of a remeshing in the case of closing the glottal channel during the oscillation period of the channel walls, the use of nonlinear elasticity models including vocal folds collision and the identification of the acoustic signal.

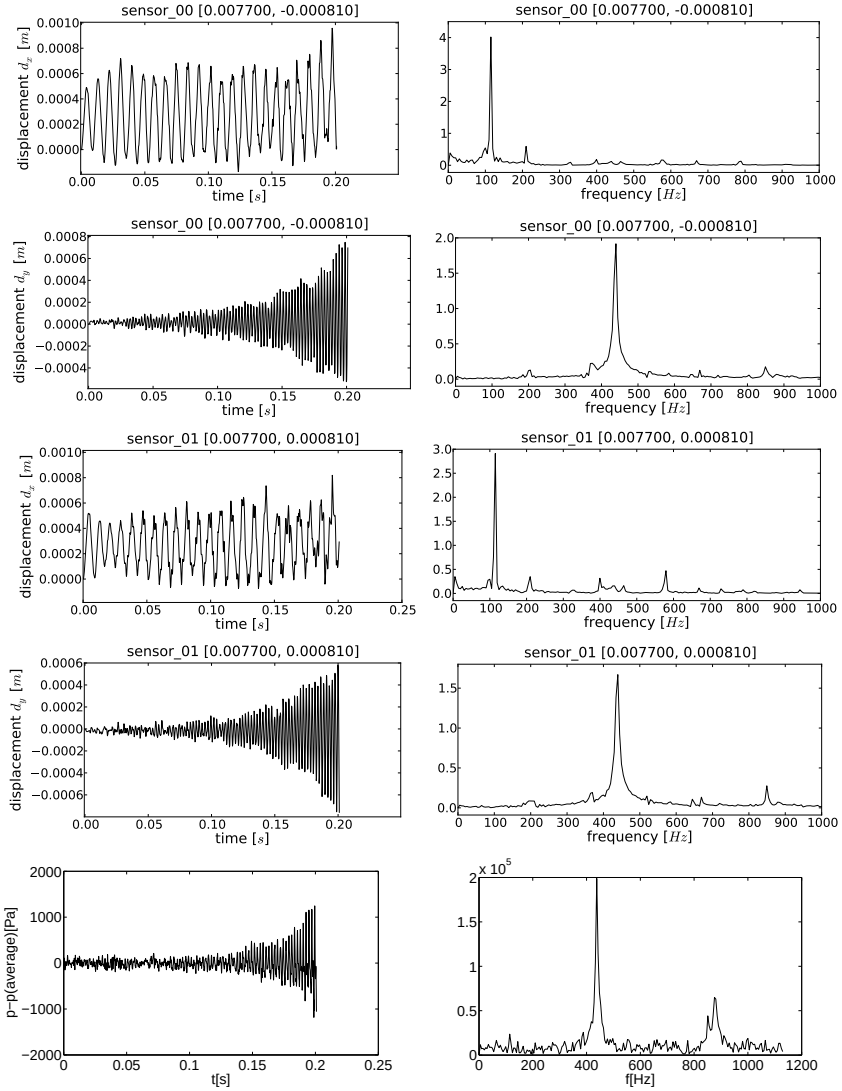

Fig. 11 Vibrations of sensor points 00 and 01 on the vocal folds and their Fourier analyses and the fluid pressure fluctuations in the middle of the gap and their Fourier analysis.

Acknowledgements This work was supported by the grants P101/11/0207 (J. Horáček), No. 201/08/0012 of the Czech Science Foundation (M. Feistauer, V.Kučera), and by the grants SVV-2012-265316 and GAChU 549912 financed by the Charles University in Prague (J. Hasnedlová-Prokopová and A. Kosík).

References

1. Fung, Y.C., An Introduction to the Theory of Aeroelaticity, Dover Publications, New York (1969)
2. Dowell, E.H., Aeroelasticity of Plates and Shells, Kluwer, Dordrecht (1974)
3. Naudasher, E. and Rockwell, D., Flow-induced vibrations, A.A.Balkema, Rotterdam (1994)
4. Dowell, E.H., A Modern Course in Aeroelaticity, Kluwer Academic Publishers (1995)
5. Bisplinghoff, R.L. and Ashley, H. and Halfman, R.L., Aeroelaticity, Dover, New York (1996)
6. Paidoussis, M.P., Fluid-Structure Interactions. Slender Structures and Axial Flow. Volume I, Academic Press, San Diego (1998)
7. Paidoussis, M.P., Fluid-Structure Interactions. Slender Structures and Axial Flow. Volume II, Academic Press, London (2004)
8. Hoffman, K.H. and Starovoitov, V.N., On a motion of a solid body in a viscous fluid. Two-dimensional case, Advanced in Mathematical Sciences and Applications, 9, 633–648 (1999)
9. Grandmont, C., Existence of a weak solutions for the unsteady interaction of a viscous fluid with an elastic plate, SIAM J. Math. Sci., 40, 716–737 (2008)
10. Guidorzi, M. and Padula, M. and Plotnikov, P.I., Hopf solutions to a fluid-elastic interaction model, Math. Models Methods Appl. Sci., 18, 215–269 (2008)
11. Neustupa, J., Existence of a weak solution to the Navier-Stokes equation in a general time-varying domain by the Rothe method, Mathematical Methods in the Applied Sciences, 32, 653–683 (2009)
12. Titze, I.R., Principles of Voice Production, National Center for Voice and Speech, Iowa City (2000)
13. Alipour, F. and Brücker, Ch. and Cook, D.D. and Gömmel, A. and Kaltenbacher, M. and Mattheus, W. and Mongeau, L. and Nauman, E. and Schwarze, R. and Tokuda, I. and Zörner, S., Mathematical models and numerical schemes for simulation of human phonation, Current Bioinformatics, 6, 323–343 (2011)
14. Horáček, J. and Šidlof, P. and Švec, J.G., Numerical simulation of self-oscillations of human vocal folds with Hertz model of impact forces, J. Fluids Struct., 20, 853–869 (2005)
15. Alipour, F. and Titze, I.R., Combined simulation of two-dimensional airflow and vocal fold vibration, P. J. Davis and N. H. Fletcher (editors): Vocal fold physiology, controlling complexity and chaos, San Diego (1996)
16. De Vries, M.P. and Schutte, H.K. and Veldman, A.E.P. and Verkerke, G.J., Glottal flow through a two-mass model: comparison of Navier-Stokes solutions with simplified models, J. Acoust. Soc. Am., 111, 1874–1853 (2002)
17. Titze, I.R., The Myoelastic Aerodynamic Theory of Phonation, National Center for Voice and Speech, Denver and Iowa City (2006)
18. Punčochářová-Pořízková, P. and Kozel, K. and Horáček, J., Simulation of unsteady compressible flow in a channel with vibrating walls - influence of frequency, Computers and Fluids, 46, 404–410 (2011)
19. Horáček, J. and Švec, J.G., Aeroelastic model of vocal-fold-shaped vibrating element for studying the phonation threshold, J. Fluids Struct., 16, 931–955 (2002)
20. Zhang, Z. and Neubauer, J. and Berry, D.A., Physical mechanisms of phonation onset: A linear stability analysis of an aeroelastic continuum model of phonation, J. Acoust. Soc. Am., 122, 2279–2295 (2007)
21. T. Nomura and T.J.R. Hughes, An arbitrary Lagrangian-Eulerian finite element method for interaction of fluid and a rigid body, Comput. Methods Appl. Mech. Engrg., 95, 115-138 (1992)
22. M. Feistauer, J. Horáček, V. Kučera, J. Prokopová, On numerical solution of compressible flow in time-dependent domains, Mathematica Bohemica (2011)
23. Badia, S. and Codina, R., On some fluid-structure iterative algorithms using pressure segregation methods. Application to aeroelasticity., Int. J. Numer. Meth. Engng., 72, 46–71 (2007)